Three dimensional in vitro models of cancer: Bioprinting multilineage glioblastoma models

Three dimensional *in vitro* models of cancer: bioprinting multilineage glioblastoma models

Miguel A Hermida[1*], Jothi Dinesh Kumar[1*], Daniela Schwarz[1], Keith G Laverty[1], Alberto Di Bartolo[1], Marcus Ardron[2], Mihails Bogomolnijs[2], Anne Clavreul[3,4], Paul M Brennan[5], Ulrich K Wiegand[6], Ferry PW Melchels[1], Will Shu[7], Nicholas R Leslie[1 #]

[1]*Institute of Biological Chemistry, Biophysics & Bioengineering, Heriot Watt University, Edinburgh, UK*
[2] *Renishaw PLC, Research Avenue North, Riccarton, Edinburgh, UK*
[3] *Département de Neurochirurgie, CHU, Angers, France*
[4] *CRCINA, INSERM, Université de Nantes, Université d'Angers, France*
[5]*Translational Neurosurgery, Centre for Clinical Brain Sciences, University of Edinburgh, Edinburgh, UK*
[6]*Queens' Medical Research Institute, University of Edinburgh, Edinburgh, UK*
[7]*Biomedical Engineering, University of Strathclyde, Glasgow, UK*

Abstract

Three dimensional (3D) bioprinting of multiple cell types within optimised extracellular matrices has the potential to more closely model the 3D environment of human physiology and disease than current alternatives. In this study, we used a multi-nozzle extrusion bioprinter to establish models of glioblastoma made up of cancer and stromal cells printed within matrices comprised of alginate modified with RGDS cell adhesion peptides, hyaluronic acid and collagen-1. Methods were developed using U87MG glioblastoma cells and MM6 monocyte/macrophages, whilst more disease relevant constructs contained glioblastoma stem cells (GSCs), co-printed with glioma associated stromal cells (GASCs) and microglia. Printing parameters were optimised to promote cell-cell interaction, avoiding the 'caging in' of cells due to overly dense cross-linking. Such printing had a negligible effect on cell viability, and cells retained robust metabolic activity and proliferation. Alginate gels allowed the rapid recovery of printed cell protein and RNA, and fluorescent reporters provided analysis of protein kinase activation at the single cell level within printed constructs. GSCs showed more resistance to chemotherapeutic drugs in 3D printed tumour constructs compared to 2D monolayer cultures, reflecting the clinical situation. In summary, a novel 3D bioprinting strategy is developed which allows control over the spatial organisation of tumour constructs for pre-clinical drug sensitivity testing and studies of the tumour microenvironment.

Keywords: 3D bioprinting, glioblastoma, cancer model, drug sensitivity, tumour microenvironment

* These authors contributed equally

To whom correspondence may be addressed. n.r.leslie@hw.ac.uk
Nick Leslie
Institute of Biological chemistry, Biophysics & Bioengineering
James Nasmyth Building, Riccarton Campus
Heriot-Watt University, Edinburgh, UK

Introduction

3D cell culture

Experiments conducted using human cells in simple adherent culture are often criticised because cells do not behave as they would in the body. On the other hand, most experiments cannot be conducted in humans and experiments conducted in mammals are expensive and often suffer criticism on ethical and scientific grounds. Therefore, as techniques to produce human cells with specific modified genomes and specific states of differentiation have progressed over recent years, the need has increased for flexible methods to recreate the numerous complex three dimensional environments within the human body. Extensive reviews have recently addressed the different approaches to the 3D culture of human cells without an adhesive substrate (Alhaque et al., 2018; Duval et al., 2017). Here we will discuss very briefly the options available for 3D cell culture and their advantages and disadvantages before focusing on 3D bioprinting as a method to develop more disease relevant tumour models and which can be used in combination with these existing approaches.

Spheroids and scaffold/matrix free 3D cultures

Perhaps the simplest forms of 3D culture are those in which cultured cells are incubated in liquid media without any adhesive substrate, encouraging them to self-aggregate. This can be achieved using either curved surfaces of materials to which cells adhere very poorly or allowing cells to settle by gravity onto an air-liquid interface in ‘hanging drop’ cultures. In these conditions, many cell types will aggregate to form dense colonies often termed spheroids and in some cases co-cultured cell types will self-organise (Fennema et al., 2013; Lazzari et al., 2018; Loessner et al., 2013; Tigyi et al., 2019). These methods provide a simple economical route to 3D cultures, and cell show gene expression patterns closer to their *in vivo* state (Chen et al., 2017), but many cell types show little or no self-aggregation and many other aspects of the in vivo environment are lacking.

Single cell or oligocellular 3D gel cultures

Techniques developed in the 1980s and 1990s have entered widespread use to study specific cell types in a more physiologically relevant environment through their simple suspension in extracellular gel matrices. This allows cells to proliferate, forming cell-cell and/or cell-matrix contacts in all orientations and in some cases develop structured 3D

mini-tissues. Ease of use has led to many experiments, particularly simple cancer cell 3D colony formation assays, being conducted in gels formed of materials not found in the human body and with which our cells do not strongly interact, such as the seaweed-derived polysaccharide agarose. However, this lack of receptor engagement of human cells with these matrices limits the usefulness of these cultures. On the other hand, the approaches most commonly used involve the suspension of cells in materials rich in mammalian extracellular matrix proteins such as collagen and laminin (e.g. Matrigel). Suspension in gels containing physiologically relevant extracellular ligands promotes gene expression patterns closer to those observed in vivo (Stankevicius et al., 2016; Tibarewal et al., 2012) and in some cases directs physiological cell polarisation and 3D tissue architectures such as the formation by epithelial cell lines of hollow acini and tubules (Berglund et al., 2013; Schmeichel and Bissell, 2003; Zegers et al., 2003).

Organoids: multipotent cell lines producing distinct spatially organised cell types.

The term organoid has been used for many decades to describe a variety of cultures and explants from different cells and organs as well as being a term used for some intracellular organelles (Simian and Bissell, 2017). As early as the 1980s, it was used to describe a colonic cell line which would differentiate into multiple cell types forming crypt-like structures in vitro (Whitehead et al., 1987). However, interest in what we now call organoids has blossomed in the last decade with the definition of procedures to consistently isolate cell lines with stem cell like properties from many healthy and diseased tissues. These cells which are multipotent *in vitro* and their methods of culture, were first optimised for intestinal epithelia. In this case, stem-like cells, either isolated as single cells or present in very small tissue fragments, give rise to spatially organised structures resembling the colonic epithelium and containing several distinct cell types (Sato et al., 2009). These cultures are termed organoids, and analogous lines, giving rise in culture to spatially organised mini-organs have now been isolated from many healthy tissue sources, including the colon, small intestine, stomach, oesophagus, pancreas, prostate, liver, brain and many other tissues (Clevers, 2016; Simian and Bissell, 2017). In addition, mutant lines can be isolated from diseased tissues, providing an excellent opportunity to model these conditions in vitro. On the other hand, in many cases the spatial organisation found in healthy tissues and often retained in the originating clinical samples appears to be lost in derived cultures.

Organoid cultures provide the opportunity to study and manipulate cells with defined genetics in vitro with much more physiological tissue organisation and gene expression profiles than previous culture approaches. Accordingly, uptake of these methods has been

very rapid, both in the study of physiology and pathology and even in drug testing. On the other hand, one drawback of these culture approaches is their reliance on poorly defined biological extracts (e.g. Matrigel) and numerous protein additives which make these experiments expensive. The cell types produced in organoid cultures are also limited to those produced by each multipotent stem cell type and therefore, for example, tumour organoids lack immune cells, vasculature and other stromal cell types.

Organotypic 3D cultures

Many other examples of complex spatially organised 3D cultures incorporating multiple cell types have been described (Shamir and Ewald, 2014). Some of these methods, such as brain slices, rely almost exclusively on the existing complex organisation of multiple cell lineages within explanted tissues. In these cases, manipulation is limited to steps such as the injection of specific exogenous cells (e.g. brain tumour cells into brain slices) or manipulation of gene expression by transfection or viral transduction of cell populations within these cultures.

Alternatively, methods such as layered skin cultures rely on the active experimental positioning of specific cell populations, potentially including defined or manipulated cells. Many of this type of organotypic culture rely on cells which will form layers in vitro replicating in vivo biology due to the experimental ease with which reproducible cultures can be prepared. A more recent extension of this approach is the use of 3D printers to position cells in more complex 3D spatial arrangements, extending the number of tissues and organs which can be prepared.

3D bioprinting

The term 3D bioprinting currently refers to the construction of three dimensional spatially designed constructs by the sequential deposition of layers of biomaterials which represent potential extracellular matrices which are either pre-mixed with live cells or are then cellularised after printing. This produces computer designed constructs containing live cells and has led to intense research in areas where specific precise 3D structure is critical, such as the manufacture of grafts of cartilage and bone for transplant surgery (Roseti et al., 2018). 3D bioprinting is currently limited by several factors. These include the need for printing biomaterials which have both the mechanical properties required for printing and the physiological properties required in printed tissues, the need to improve the resolution of printing, in terms of the smallest features or domains with a construct and also the current inability to introduce appropriate vasculature within constructs. However,

there is great research interest in the potential of 3D bioprinting to provide flexible hardware and methods to rapidly generate many different user-defined diverse spatially detailed 3D cultures containing numerous different cell types and matrices (Heinrich et al., 2019). Bioprinting also provides opportunities for automation and the production of large numbers of replicate 3D models for basic science and for drug testing. Therefore it seems likely to be an increasingly common practice, and importantly, bioprinting technology can be combined with the approaches above, e.g. printing spheroids or fabricating organotypic cultures. Notably, the first studies combining the self-organising capabilities of organoids with the operator designed possibilities of bioprinting are emerging (Reid et al., 2018).

Experimental models of Glioblastoma

Brain tumours as a group have amongst the worst outcomes of any type of cancer (Quaresma et al., 2015). This is particularly true of glioblastoma, the most common malignant adult brain cancer, with 10 year survival rates below 1% (Tykocki and Eltayeb, 2018). Improving the treatment of glioblastoma is made more difficult both by the lack of pre-clinical experimental systems which accurately predict drug responses in patients and by poor understanding of the complex multicomponent environment within these tumours. Both problems motivate efforts to develop better disease models and given the challenges of minimising suffering caused by tumour growth in the brain of study animals, there is a strong push towards in vitro models.

Glioblastomas contain cancer stem cells and more differentiated cancer cells with less capacity for self-renewal (Chen et al., 2012; Jackson et al., 2015; Singh et al., 2003). These tumours also contain stromal cells such as microglia and other macrophages, microvascular endothelial cells and glioblastoma-associated stromal cells within a complex heterogeneous extracellular matrix (Barros et al., 2011; Charles et al., 2012; Clavreul et al., 2014). In many tumour types including glioblastoma, it appears that tumour stromal cells and the acellular components of the tumour niche modulate tumour development and drug responses (Charles et al., 2012; Cheng et al., 2013; Shi et al., 2017). Therefore, pharmaceutical targeting of these microenvironmental compartments, including efforts to enhance the immune destruction of cancer cells, is becoming a major strategy in the treatment of many cancers such as glioblastoma (Boussiotis and Charest, 2018; Guerra et al., 2018; Kurz and Wen, 2018; Valkenburg et al., 2018).

The importance of three-dimensional models to study cancer biology and drug responses has been clear for a long time, with numerous studies deriving data from 3D culture which are closer to clinical data and animal data than those derived from adherent cell cultures

(Schmeichel and Bissell, 2003; Xu et al., 2014; Yamada and Cukierman, 2007). Cell morphology, cell-cell and cell-matrix interaction, cell signalling, gene expression (Chen et al., 2017; Ramos et al., 2018), differentiation and drug responses are all frequently different in 2D and 3D cultures (Baker and Chen, 2012; Jhanwar-Uniyal et al., 2013; Jhanwar-Uniyal et al., 2019; Thoma et al., 2014). Additionally, in the rare cases in which adherent cell culture models incorporate stromal cells and extracellular matrix components, the way in which these factors interact with tumour cells is very different in 2D monolayers from circumstances in vivo or in 3D culture.

3D printing, also termed additive manufacture, is the sequential deposition of layers of material at specified positions to build potentially complex 3D structures. In recent years there has been substantial interest in the 3D printing of live cells as a potential solution to the flexible creation of diverse engineered tissues both for regenerative/reparative medicine and to generate custom disease models (Derby, 2012; Knowlton et al., 2015; Murphy and Atala, 2014). 3D printing live cells within an optimised extracellular matrix (bioprinting) can provide high spatial precision in the non-uniform deposition of multiple cells and matrix components and additionally allows high cell densities and construct reproducibility. The first application of this method using cancer cells was the 3D bioprinting of Hela cell constructs in 2014 (Zhao et al., 2014) but other studies have followed (Dai et al., 2016; Jiang et al., 2017).

Several 3D bioprinting hardware platforms have been developed each with advantages and limitations which have been recently reviewed (Li et al., 2016). Here we have further developed our recent extrusion printing method (Tabriz et al., 2015) and applied this to produce multilineage glioblastoma models. This robust and flexible 3D bioprinting strategy allows the testing of drug sensitivity and the analysis of stromal cell influence on tumor cell signaling at the single level through the use of fluorescence protein kinase reporters.

Materials and Methods

Bioink preparation

G-rich alginate powder (Protanal LF 10/60 FT, FMC Biopolymers) as well as RGDS-Alginate were sterilised by exposure to UV light for 3 hours. Cross-linking reagents, $CaCl_2$ and $BaCl_2$ (Sigma Aldrich, Gillingham, Dorset, UK) were prepared in milliQ water adjusting the osmolarity of each solution to 330 mOsm/L and pH to 7.4. Cross-linking solutions were sterilised by filtering.

Alginate modification

RGDS-Alginate was synthesised using carbodiimide chemistry based on previous publications (Rowley et al., 1999). Briefly, a 1% solution of alginate in 100 mM MES, pH6.8 was activated using 10 mM Sulfo-NHS (Sigma Aldrich) and 9 mM EDC (Alfa Aesar). Then, RGDS peptide (Alfa Aesar, Heysham, UK) was added (0.01% w/v or 1% of alginate mass) and the reaction stirred for 1 h. The solution was then dialysed against Milli-Q water using a 3.5 kDa MW membrane cassette (Thermo Fisher, Loughborough, UK) for 3 days with 8 water changes. After dialysis, RGDS-Alginate was precipitated by adding ethanol to 70% volume and washed several times with more ethanol. The modified alginate was then further purified by treating it with chloroform and activated charcoal. The solid was then freeze dried. The same reaction was performed for fluorescein alginate by adding 10 mM 5-aminofluorescein (Sigma Aldrich) in place of the RGDS peptide. Purity of alginate, G/M ratio and conjugation efficiency were assessed using 1H-NMR in a Bruker AVIII400 with water suppression; high power 1H pulse of 10 µs at -1.83 dB; number of scans 256 with a relaxation delay of 1 s and acquisition time of 1 s. Line broadening 1 Hz.

Dynamic mechanical analysis

3D hydrogel structures with a diameter of 3±0.5 mm and a height of 5±0.5 mm was prepared from 400 µL of printing material, consisting of specific percentages of RGD-alginate, hyaluronic acid **(**Thermo Fisher) and collagen-1 (Collagen Solutions, Glasgow, UK) with 10,000 cell/ µL. Calcium chloride (0 - 50 mM) was used as crosslinking agent for 3 minutes. Compression tests were performed in triplicate on a 2980 DMA (TA Instruments, New Castle, DE, USA) with a ramp force from 0.1–1 N for 10 min, at room temperature. The elastic modulus was calculated as the slope of the stress-strain curve that was obtained from the compression test.

3D Bioprinting

3D bioprinting was performed by extrusion using either a modified open-source Fab@Home dual syringe printer (Tabriz et al., 2015) or a pre-prototype extrusion bioprinter provided by Renishaw PLC (Edinburgh, UK), with an 8-valve syringe pump and a single print head mounted with up to 6 extrusion delivery lines and nozzles that can deposit up to 6 different independent bioinks or materials required for bioprinting, such as divalent cation solutions. Unless specified, a 200 μm diameter steel conical nozzle was used. A hydrophobic and conical nozzle promoted consistent deposition while minimising the shear stress on the cells being ejected.

Cell culture

In this study, prior to printing, cells were grown in standard adherent cell culture. Human glioblastoma (U87MG, ECACC) and monocytic (MM6, Mono-Mac-6, David Brown; School of Life Sciences, Heriot-Watt University) cell lines were cultured in minimum essential medium (MEM) supplemented with 10% (v/v) foetal bovine serum (FBS), 2 mM L-glutamine, 1x non-essential amino acid mix (NEAA, Gibco Thermo-Fisher), and 1 mM sodium pyruvate. Human embryonic kidney 293T (HEK293T), MDA-MB-231, MDA-MB-468, 1321N1 and FLO-1 cells were maintained in Dulbecco Modified Essential Medium (DMEM) supplemented with 10% (v/v) FBS, 2 mM L-Glutamine, 1x NEAA and 1 mM sodium pyruvate. OE33 and DBTRG.05MG cells were maintained in RPMI 1640 medium supplemented with 2mM glutamine and 10% FBS. Glioblastoma stem cell line (G7, G144 and G166, provided by Steve Pollard; MRC Centre for Regenerative Medicine, University of Edinburgh (Pollard et al., 2009)) were cultured in DMEM F-12 (Sigma Aldrich) supplemented with 8 mM glucose (Sigma Aldrich), 1x NEAA (Gibco Thermo Fisher), Pen-strep, 30 mg/mL Bovine Serum Albumin Fraction V, 100 μM beta-mercaptoethanol, neuronal cell culture supplements B27 0.5X and N2 0.5X (Thermo Fisher Scientific) , 10 ng/mL murine Epidermal Growth Factor and human Fibroblast Growth Factor (Peprotech, London W6, UK) and 1 μg/mL laminin (Sigma Aldrich). Human GASCs were provided by Anne Clavreul (Département de Neurochirurgie, CHU d'Angers, Angers, France) and cultured as previously described (Clavreul et al., 2014). Human microglia were purchased from Celprogen and were cultured in human microglia primary cell culture complete media with serum (Celprogen, York, UK). In order to activate MM-6 cells, cells were exposed to 50 ng/mL of 12-O-Tetradecanoylphorbol 13-acetate (PMA; Sigma Aldrich) overnight. After 24 h the cells became adherent and PMA was removed. Cells were incubated for another 2 days and then trypsinised for bioprinting.

Imaging of the cells was performed using either a Confocal Laser Scanning Microscope (Leica SP5 SMD, Leica microsystems, ESRIC imaging facility, HWU) or a modified Nikon

two-photon microscope (CALM facility, University of Edinburgh). Data was analysed using Imaris software (Bitplane, Belfast, UK).

Cell line modification

Cells lines were modified to express fluorescent proteins and reporters by lentiviral transduction. cDNAs encoding fluorescent proteins were subcloned into the BamHI and NotI sites of the lentiviral vector pHR-SIN (Demaison et al., 2002; Ikeda et al., 2003). Kinase biosensors for ERK, p38, PKA and JNK expressed from lentiviral vectors (Regot et al., 2014) were supplied by Addgene (IDs: 59150, 59152, 59153, and 59151 respectively). Lentiviral particles were generated using the respective plasmid of interest co-transfected into HEK293T cells alongside a vector encoding the VSV-G envelope glycoprotein and pCMV ΔR8.2 lentiviral packaging construct. Triple transfection used TransIT LT1 (Mirus, Cambridge Bioscience, Cambridge, UK) reagent and supernatant containing viral particles was collected after 3 days. Target cells were transduced using this viral supernatant and Polybrene (Sigma Aldrich) at 1.6 μg/mL concentration. Cells were either used as oligoclonal populations or subsequently cell lines were selected by puromycin selection.

Cell proliferation and viability

Resazurin (7-Hydroxy-3H-phenoxazin-3-one-10-oxide sodium salt, Sigma Aldrich) was used to determined cell numbers as follows. Resazurin stock solution was added into the cell medium at a final concentration of 44 μM. After 3-4 h, fluorescence was measured using a plate reader, with excitation at 570 nm and detecting emission at 590 nm. Autoclaved resazurin (resorufin) was used as a reduced control, resazurin in medium as the oxidised control. Blanks and calibration curves were also included in every plate to assure the specificity and linearity of response. Each condition was measured in triplicate and data presented as mean +/- SD. To study the viability of the 3D printed cells, propidium iodide (PI, Sigma) was added to the media at a final 2.5 μM concentration and incubated for 30 min in the dark at 37 °C. Nuclear staining of PI was measured by Confocal Laser Scanning Microscope Leica SP5 SMD (CLSM, Leica microsystems, ESRIC facility). A ratio of apoptotic cells (red) to total cell number was estimated using the image analysis software Imaris (Bitplane) for each stack. In some experiments, specifically GFP-expressing fluorescent cells were analysed within co-cultured cell mixtures. PI concentration was optimised by using the cytotoxic agent etoposide (Sigma Aldrich) at a final 10 μM concentration to assure that the dead cell staining is efficient in the alginate gel.

Single cell protein kinase activity analysis

The kinase translocation reporters pLentiPGK Puro DEST ERK KTR Clover, pLentiPGK Puro DEST JNK KTR Clover, pLentiPGK Puro DEST p38 KTR Clover and pLentiPGK Puro DEST PKA KTR Clover (Regot et al., 2014), were made by Markus Covert's laboratory (Addgene plasmids # 59150, 59151, 59152 and 59153 respectively). The plasmids were incorporated into second generation lentiviral particles and cells were transduced using polybrene (Sigma Aldrich) and selected for plasmid incorporation (puromycin 500 ng/mL for 6 days). The fluorescently labelled cells were imaged and ratio nuclear/cytoplasmic signal was calculated using ImageJ. At least 30 cells were randomly selected per condition.

Recovery of cellular protein and RNA from 3D printed cultures

3D alginate cultures were washed with ice cold PBS and treated with 7x gel volume of pre-chilled chelating agent to sequester divalent cations and dissolve each gel. The chelating agents used were EDTA, EGTA or sodium citrate. The resultant culture mixtures were incubated on ice for 10 minutes then centrifuged at 4°C and cell pellets lysed for the analysis of protein and RNA following previously published methods (Davidson et al., 2010; Tibarewal et al., 2012).

Drug sensitivity testing

Cells were printed in RGDS-alginate on coverslips and transferred into well plates having a 2D control using the 3D-printer. Constructs were then exposed to calcium crosslinking and incubated for 24 h. Cells were then exposed to specific concentrations of cisplatin (Cayman chemicals, Ann Arbor, MI, USA) and temozolomide (Abcam, Cambridge, UK). Drug stock solutions were made using NaCl 0.9% and sterile DMSO respectively and cisplatin sterilised by filtering. The different drug concentrations were added and left for 72 hours, then, cell number was assessed using resazurin as previously described. Each experimental point was done at least in triplicate.

Results

Optimising matrices for 3D bioprinting glioblastoma cells

In this study, 3D bioprinting methods were developed to print cell-laden structures in a matrix composed largely of modified alginate. The printer used was a prototype extrusion bioprinter provided by Renishaw (Fig. 1B, C). Prior to printing, one or more cell populations prepared in adherent culture were mixed into alginate matrices which were partially cross-linked with a low $CaCl_2$ concentration (<5 mM). For some experiments, other matrix components such as collagen or hyaluronic acid were incorporated as minority components (<250 mg/ml). Cells and matrices were rapidly printed (10 minutes – 1 hour) followed by final cross-linking with higher concentrations of $CaCl_2$ or $BaCl_2$ for 15 min (Figure 1A, 2A-C). Increasing concentration of $CaCl_2$ generated higher stiffness of 2% alginate gels, with exposure to 10 mM $CaCl_2$ giving a mean stiffness of 11.9 kPa and 50 mM of 25.7 kPa (Fig. 2B and 2C).

11.9 kPa is at the higher end of the range of stiffness measurements made on tissue samples from both glioblastomas and normal brain (Bouchonville et al., 2016; Niu et al., 2015; Streitberger et al., 2014). We have previously shown the extended invasive morphology of U87MG cells suspended in Matrigel (Davidson et al., 2010; Tibarewal et al., 2012). To investigate the effects of alginate crosslinking on cell morphology, we suspended U87MG cells in a matrix made up of 50% matrigel and final 2% (w/v) RGD-alginate and applied a range of calcium ion crosslinking concentrations. These experiments showed that an increase in matrix cross-linking significantly decreased cell spreading and elongation, possibly due to ‘caging in’ by a surrounding densely crosslinked matrix (Fig. 2D, 2E) and we elected to use 10mM $CaCl_2$ crosslinking in later printing experiments.

One advantage of alginate over other 3D cell culture matrices is the ability to liquify the matrix using chelating agents and recover cells for protein analysis within timescales of a few minutes. This contrasts with e.g. matrigel and should allow the retention of many post-translational protein modifications (Lee et al., 2007; Tibarewal et al., 2012). To confirm this, RNA and protein were analysed in samples of U87MG cells recovered from 3D alginate cultures and from control adherent cultures (Fig. 3). This analysis showed that phosphorylation of two sites, Thr308 and Ser473, on the oncogenic protein kinase AKT was retained in all of these samples, particularly after recovery in EGTA.

Furthermore, we saw highly reproducible recovery of cellular RNA analysed by quantitative RT-PCR (Fig. 3).

Bioprinting diverse cell types in modified alginate

There is little or no evidence that any human cell type shows receptor-mediated engagement with alginate. Accordingly, human cell types which take up extend morphologies in vivo instead retain a spherical morphology after deposition within even soft alginate matrices with low crosslinking density (Ning et al., 2018; Tabriz et al., 2015). To avoid the non-physiological retention of a spherical morphology within the alginate matrix, we chemically modified the alginate polymer using carbodiimide conjugation to attach an Arg-Gly-Asp peptide sequence (RGD) which is present in many extracellular matrix proteins and is bound by several members of the integrin class of cell-surface adhesion receptors (Rowley et al., 1999). The comparison of U87MG glioblastoma cells and activated MM6 cells bioprinted within unmodified alginate and in RGD-alginate showed cell spreading and apparent adhesion in less than 24 hours only within RGD-alginate (Fig. 4A, B). U87MG cells could be maintained in RGD-alginate matrice whith very high viability and proliferate in culture for more than a month (Fig. 4C, D). Therefore, RGD-alginate was used in all further experiments unless noted.

It is recognised that increased shear stress in viscous matrices during printing increases cell death (Derby, 2012; Heinrich et al., 2019). As previously seen, in matrices crosslinked during and after printing, U87MG cells could be printed within unmodified alginate matrices with very high viability and proliferate in culture for more than a month (Figure 4C, D) (Tabriz et al., 2015). To test whether other cell types retained viability after 3D bioprinting, we used propidium iodide exclusion to detect cell death after bioprinting of a range of established cell lines in RGD-alginate (Fig. 4E and Fig. 8D). Experimental reproducibility and cell viability >90% was seen with glioblastoma cells (U87-MG, DBTRG, and 1231N1), and oesophageal adenocarcinoma (OE33, FLO-1) and breast cancer (MDA MB-231) cells. Only one breast cancer cell line, MDA-MB-468 which is unusually sensitive to EGF-induced apoptosis (Jackson and Ceresa, 2016), showed slightly lower viability but still >80%.

Modelling the glioblastoma tumour microenvironment

The tumour microenvironment of glioblastoma, as with almost all cancers, contains alongside neoplastic cancer cells, large numbers of diverse cell types which influence tumour biology and drug sensitivity (Barcellos-Hoff et al., 2013; Charles et al., 2012; McMillin et al., 2013). To test our ability to more closely reproduce the complexity of the tumour microenvironment by co-printing multiple cell types, we printed U87-MG cells together with WI-38 non-immortalised fibroblasts and the macrophage-like Mono-Mac-6

(MM6) cell line, each expressing a distinct fluorescent protein (yellow, blue and red respectively), within an RGD-alginate matrix (Fig. 4F).

Work to identify tumour repopulating stem cells in glioblastoma has provided patient derived cell lines which share many gene expression markers with neural stem cells and which closely recapitulate human glioblastoma progression when orthotopically xenografted in in mice (Pollard et al., 2009). The suitability of these Glioblastoma Stem Cells (GSCs) for bioprinting in RGD-alginate using our method was tested first by assessing the viability post printing of these cells by propidium iodide exclusion. Three different GSC lines, G144, G166 and G7 (Pollard et al., 2009), all showed viability higher than 90% (Fig. 5A) and there was no indication of reduced viability after exposure to the divalent cation cross-linkers, calcium and barium. Next, we investigated whether the printing process and subsequent culture of these cells in RGD-alginate resulted in an increase in the differentiation of these GSC indicating a loss of pluripotency. For this, GSCs were cultured for 7 days with and without EGF and FGF either in adherent culture or bioprinted in RGD-alginate. As previously described, growth factor withdrawal caused the expression of the glial lineage marker GFAP and the loss of the expression of the pluripotency marker Nestin in 2D cultures (Fig. 5). However, the 3D bioprinted GSC did not show any loss in nestin expression and did not express GFAP, even following growth factor withdrawal (Fig. 5B), suggesting that the bioprinting of these cells promotes the maintenance of at least some GSC characteristics.

Bioprinting GSCs in combination with both patient-derived GASCs and with human microglia had no adverse effects on cell viability of these cell types (Charles et al., 2012; Clavreul et al., 2014) (Fig. 5C).

Drug sensitivity in 3D bioprinted cancer cells and 2D adherent culture

U87MG and G7 cells were each cultured alone in both adherent culture and 3D printed in multiple well plates using RGD-modified alginate matrix. Cells were exposed to increasing concentrations of either cisplatin or temozolomide and viability assessed using resazurin (Fig. 6A, B). In 2D adherent cultures, the front line glioblastoma drug temozolomide reduced cell numbers with IC_{50} values of 928.7±1.0 μM and 333.3±1.1 μM for U87MG and G7 respectively. When the cells were bioprinted in 3D, the temozolomide IC_{50} values increased by slightly more than two fold to 1994±1.0 μM and 748.8±1.1 μM respectively. We then tested the DNA damaging agent cisplatin. This showed that U87MG and G7 have similar cisplatin IC50s of 8.94±1.09 μM and 10.0±1.1 μM respectively in 2D adherent cultures. However, the 3D bioprinted cultures show a significant resistance to cisplatin, with an IC50 of 69.8±1.1 μM (U87MG) and 241±1.1 μM (G7). These results show that the

3D bioprinted constructs are very strongly resistance to cisplatin, a drug which has failed in several clinical trials for glioblastoma (EORTC, 1991; Grossman et al., 2003).

Next, we aimed to test how incorporating macrophage-like stromal cells within the 3D printed constructs affected drug sensitivity. Either G7 or U87MG cells were 3D printed with and without 20% by cell number MM6 cells, PMA-activated MM6 (aMM6) or human microglia mixed with the glioblastoma cells. The bioprinted structures were then treated with IC_{50} concentrations of temozolomide or vehicle and viability assessed by DRAQ7 staining and microscopy. This data shows that for U87MG, the presence of MM6 decrease the sensitivity of the drug, with the surviving fraction increasing from 50.1±6.7% to 73.8±5.2%. On the other hand, aMM6 did not decrease the sensitivity to temozolomide, maintaining the surviving fraction in 53.1±6.7%. G7 cells however, did not display this effect, with temozolomide sensitivity increasing modestly when they were co-printed with MM6, with cell surviving fraction decreasing from 56.0±3.53 % to 41.9±5.75 %. Similarly to U87MG, aMM6 did not significantly alter the surviving fraction, which remained 57.1±6.8 %. When primary human microglia were co-printed with the G7 cells, the percentage of viable cells did not significantly change relative to only G7, suggesting that the choice of relevant stromal cells can impact substantially on the outcome of these experiments.

Single cell protein kinase activation analysis

As a tool to study cell signalling at the single cell level, protein kinase reporters were used to assess the activity of the ERK protein kinases (Figure 7) as well as p38, JNK and PKA (data not shown). These previously described biosensors are based on fluorescence translocation driven by their phosphorylation by specific protein kinases, with specificity provided both by phosphorylation site sequence specificity and independently by kinase docking sites within each reporter. They display fluorescence in the nucleus when the reporter is unphosphorylated due to low kinase activity and display fluorescence in the cytoplasm when the reporter is phosphorylated due to higher kinase activity (Regot et al., 2014).

Figure 7A shows the behaviour of U87MG cells expressing the ERK KTR mClover biosensor, which appeared similarly concentrated in the cytoplasm and nucleus of most cells growing in 10% FBS. We observed a fluorescence translocation when cells were cultured in serum free medium, with fluorescence being nuclear in most cells. Conversely, when cells were exposed to medium with 20% FBS most cells displayed a largely cytoplasmic localisation of the reporter. To assess the kinase activity in a co-culture of glioblastoma cells with MM6 cells, polyclonal populations of U87MG cells expressing ERK-KTR-mClover were incubated either in adherent culture or 3D bioprinted either alone

or in combination with MM6 or aMM6 cells. Images were taken using a two photon microscope and fluorescence ratio between nuclear and cytoplasmic fluorescence measured (Fig. 7B). This showed that biosensor analysis in these 3D printed constructs indicates an increase in the activation status of the ERK kinases when the cells were co-printed with aMM6 or with MM6. This ability to analyse signalling in individual printed cells supports the expectation that the presence of stromal cells can activate cell signalling pathways in 3D co-printed constructs.

Finally, in testing more complex spatial arrangements within printed constructs, tumour cells were positioned centrally with a surrounding layer of mixed tumour and stromal cells. Two-layered and three-layered structures were 3D printed using the sequential cross-linking method and modified alginate (Figure 8A, B). This was reproducible when bioprinting multiple well plates and also showed that the same number of cells can be deposited when compared to deposition of a cell suspension on plastic with only marginally higher variability in cell number (Fig. 8C and 8D).

Discussion

We present 3D bioprinting methods using bioinks based upon modified alginate to prepare tumour models incorporating tumour and stromal cells from glioblastoma. We show that crosslinking alginate with higher concentrations of divalent cations which should have benefits in terms of structural integrity and resolution can inhibit cell spreading and cell-cell interaction leading to unphysiological results. For this reason, and due to the lower stiffness of brain tumour tissue (mostly in the range 1-10 kPa (Bouchonville et al., 2016; Niu et al., 2015; Streitberger et al., 2014)), we concentrated on the use of lower concentrations of alginate and cross-linker, generally 2% alginate and 10mM Ca^{2+}. Similarly, to improve cell-cell interaction, we used RGD-peptide conjugated alginate, and in some cases additional hyaluronic acid, to promote the engagement of cells with the surrounding matrix.

When the 3D bioprinted glioblastoma cell constructs were used to test sensitivities to temozolomide and cisplatin, a modest drug resistance relative to adherent culture was observed for temozolomide, but a very substantial resistance for cisplatin (Figure 6). Relating to this data, it is notable that cisplatin was previously put through several clinical trials for high grade glioma without success, but gives promising cytotoxicity data in 2D and some 3D cultures, including collagen gels and 3D spheroids/neurospheres (Ahmed et al., 2018; Berger et al., 2018; Yuki et al., 1994; Yung et al., 1982). Investigation into the factors which contribute to this cisplatin resistance in 3D bioprinted culture may help inform future 3D culture models of glioblastoma.

Whilst attempting to develop standardized cultured cell-based models which more closely represent healthy and diseased tissue, the impact and value of some modified characteristics of the model are often unclear without e.g. impractical deep gene expression analysis. However, as more highly evolved models are produced and better characterisation of these models is performed, it should be possible cost-effectively to match individual models to individual applications. The methods described here, which support the spatial organisation of multiple cell types which contribute to the glioblastoma environment and allow recovery of protein and RNA as well as analysis of signalling at the single cell level, should accelerate the provision of improved models of glioblastoma.

Declarations of interest

MA and MB are full time employees of Renishaw PLC.

Acknowledgements

This work was funded by a New Ideas project grant from the Brain Tumour Charity (GN-000344). MAH was supported by a Heriot Watt University James Watt Scholarship. We thank Steven Pollard (University of Edinburgh) for the kind provision of Glioma Stem Cell lines...

References

References

Ahmed, E.M., Bandopadhyay, G., Coyle, B., Grabowska, A., 2018. A HIF-independent, CD133-mediated mechanism of cisplatin resistance in glioblastoma cells. Cell Oncol (Dordr) 41(3), 319-328.
Alhaque, S., Themis, M., Rashidi, H., 2018. Three-dimensional cell culture: from evolution to revolution. Philos Trans R Soc Lond B Biol Sci 373(1750).
Baker, B.M., Chen, C.S., 2012. Deconstructing the third dimension: how 3D culture microenvironments alter cellular cues. J Cell Sci 125(Pt 13), 3015-3024.
Barcellos-Hoff, M.H., Lyden, D., Wang, T.C., 2013. The evolution of the cancer niche during multistage carcinogenesis. Nat Rev Cancer 13(7), 511-518.
Barros, C.S., Franco, S.J., Muller, U., 2011. Extracellular matrix: functions in the nervous system. Cold Spring Harb Perspect Biol 3(1), a005108.
Berger, G., Grauwet, K., Zhang, H., Hussey, A.M., Nowicki, M.O., Wang, D.I., Chiocca, E.A., Lawler, S.E., Lippard, S.J., 2018. Anticancer activity of osmium(VI) nitrido complexes in patient-derived glioblastoma initiating cells and in vivo mouse models. Cancer Lett 416, 138-148.
Berglund, F.M., Weerasinghe, N.R., Davidson, L., Lim, J.C., Eickholt, B.J., Leslie, N.R., 2013. Disruption of epithelial architecture caused by loss of PTEN or by oncogenic mutant p110alpha/PIK3CA but not by HER2 or mutant AKT1. Oncogene 32(37), 4417-4426.
Bouchonville, N., Meyer, M., Gaude, C., Gay, E., Ratel, D., Nicolas, A., 2016. AFM mapping of the elastic properties of brain tissue reveals kPa mum(-1) gradients of rigidity. Soft Matter 12(29), 6232-6239.
Boussiotis, V.A., Charest, A., 2018. Immunotherapies for malignant glioma. Oncogene 37(9), 1121-1141.
Charles, N.A., Holland, E.C., Gilbertson, R., Glass, R., Kettenmann, H., 2012. The brain tumor microenvironment. Glia 60(3), 502-514.
Chen, H., Seaman, L., Liu, S., Ried, T., Rajapakse, I., 2017. Chromosome conformation and gene expression patterns differ profoundly in human fibroblasts grown in spheroids versus monolayers. Nucleus 8(4), 383-391.
Chen, J., Li, Y., Yu, T.S., McKay, R.M., Burns, D.K., Kernie, S.G., Parada, L.F., 2012. A restricted cell population propagates glioblastoma growth after chemotherapy. Nature 488(7412), 522-526.
Cheng, L., Huang, Z., Zhou, W., Wu, Q., Donnola, S., Liu, J.K., Fang, X., Sloan, A.E., Mao, Y., Lathia, J.D., Min, W., McLendon, R.E., Rich, J.N., Bao, S., 2013. Glioblastoma stem cells generate vascular pericytes to support vessel function and tumor growth. Cell 153(1), 139-152.
Clavreul, A., Guette, C., Faguer, R., Tetaud, C., Boissard, A., Lemaire, L., Rousseau, A., Avril, T., Henry, C., Coqueret, O., Menei, P., 2014. Glioblastoma-associated stromal cells (GASCs) from histologically normal surgical margins have a myofibroblast phenotype and angiogenic properties. J Pathol 233(1), 74-88.
Clevers, H., 2016. Modeling Development and Disease with Organoids. Cell 165(7), 1586-1597.
Dai, X., Ma, C., Lan, Q., Xu, T., 2016. 3D bioprinted glioma stem cells for brain tumor model and applications of drug susceptibility. Biofabrication 8(4), 045005.
Davidson, L., Maccario, H., Perera, N.M., Yang, X., Spinelli, L., Tibarewal, P., Glancy, B., Gray, A., Weijer, C.J., Downes, C.P., Leslie, N.R., 2010. Suppression of cellular proliferation and invasion by the concerted lipid and protein phosphatase activities of PTEN. Oncogene 29(5), 687-697.
Demaison, C., Parsley, K., Brouns, G., Scherr, M., Battmer, K., Kinnon, C., Grez, M., Thrasher, A.J., 2002. High-level transduction and gene expression in hematopoietic repopulating cells using a human immunodeficiency virus type 1-based lentiviral vector containing an internal spleen focus forming virus promoter. Hum Gene Ther 13(7), 803-813.
Derby, B., 2012. Printing and prototyping of tissues and scaffolds. Science 338(6109), 921-926.
Duval, K., Grover, H., Han, L.H., Mou, Y., Pegoraro, A.F., Fredberg, J., Chen, Z., 2017. Modeling Physiological Events in 2D vs. 3D Cell Culture. Physiology (Bethesda) 32(4), 266-277.

EORTC, 1991. Cisplatin does not enhance the effect of radiation therapy in malignant gliomas. EORTC Brain Tumor Group. Eur J Cancer 27(5), 568-571.
Fennema, E., Rivron, N., Rouwkema, J., van Blitterswijk, C., de Boer, J., 2013. Spheroid culture as a tool for creating 3D complex tissues. Trends Biotechnol 31(2), 108-115.
Grossman, S.A., O'Neill, A., Grunnet, M., Mehta, M., Pearlman, J.L., Wagner, H., Gilbert, M., Newton, H.B., Hellman, R., Eastern Cooperative Oncology, G., 2003. Phase III study comparing three cycles of infusional carmustine and cisplatin followed by radiation therapy with radiation therapy and concurrent carmustine in patients with newly diagnosed supratentorial glioblastoma multiforme: Eastern Cooperative Oncology Group Trial 2394. J Clin Oncol 21(8), 1485-1491.
Guerra, D.A.P., Paiva, A.E., Sena, I.F.G., Azevedo, P.O., Silva, W.N., Mintz, A., Birbrair, A., 2018. Targeting glioblastoma-derived pericytes improves chemotherapeutic outcome. Angiogenesis.
Heinrich, M.A., Liu, W., Jimenez, A., Yang, J., Akpek, A., Liu, X., Pi, Q., Mu, X., Hu, N., Schiffelers, R.M., Prakash, J., Xie, J., Zhang, Y.S., 2019. 3D Bioprinting: from Benches to Translational Applications. Small 15(23), e1805510.
Ikeda, Y., Takeuchi, Y., Martin, F., Cosset, F.L., Mitrophanous, K., Collins, M., 2003. Continuous high-titer HIV-1 vector production. Nat Biotechnol 21(5), 569-572.
Jackson, M., Hassiotou, F., Nowak, A., 2015. Glioblastoma stem-like cells: at the root of tumor recurrence and a therapeutic target. Carcinogenesis 36(2), 177-185.
Jackson, N.M., Ceresa, B.P., 2016. Protein Kinase G facilitates EGFR-mediated cell death in MDA-MB-468 cells. Exp Cell Res 346(2), 224-232.
Jhanwar-Uniyal, M., Jeevan, D., Neil, J., Shannon, C., Albert, L., Murali, R., 2013. Deconstructing mTOR complexes in regulation of Glioblastoma Multiforme and its stem cells. Adv Biol Regul 53(2), 202-210.
Jhanwar-Uniyal, M., Wainwright, J.V., Mohan, A.L., Tobias, M.E., Murali, R., Gandhi, C.D., Schmidt, M.H., 2019. Diverse signaling mechanisms of mTOR complexes: mTORC1 and mTORC2 in forming a formidable relationship. Adv Biol Regul 72, 51-62.
Jiang, T., Munguia-Lopez, J.G., Flores-Torres, S., Grant, J., Vijayakumar, S., Leon-Rodriguez, A., Kinsella, J.M., 2017. Directing the Self-assembly of Tumour Spheroids by Bioprinting Cellular Heterogeneous Models within Alginate/Gelatin Hydrogels. Sci Rep 7(1), 4575.
Knowlton, S., Onal, S., Yu, C.H., Zhao, J.J., Tasoglu, S., 2015. Bioprinting for cancer research. Trends Biotechnol 33(9), 504-513.
Kurz, S.C., Wen, P.Y., 2018. Quo Vadis-Do Immunotherapies Have a Role in Glioblastoma? Curr Treat Options Neurol 20(5), 14.
Lazzari, G., Nicolas, V., Matsusaki, M., Akashi, M., Couvreur, P., Mura, S., 2018. Multicellular spheroid based on a triple co-culture: A novel 3D model to mimic pancreatic tumor complexity. Acta Biomater 78, 296-307.
Lee, G.Y., Kenny, P.A., Lee, E.H., Bissell, M.J., 2007. Three-dimensional culture models of normal and malignant breast epithelial cells. Nat Methods 4(4), 359-365.
Li, J., Chen, M., Fan, X., Zhou, H., 2016. Recent advances in bioprinting techniques: approaches, applications and future prospects. J Transl Med 14, 271.
Loessner, D., Little, J.P., Pettet, G.J., Hutmacher, D.W., 2013. A multiscale road map of cancer spheroids--incorporating experimental and mathematical modelling to understand cancer progression. J Cell Sci 126(Pt 13), 2761-2771.
McMillin, D.W., Negri, J.M., Mitsiades, C.S., 2013. The role of tumour-stromal interactions in modifying drug response: challenges and opportunities. Nat Rev Drug Discov 12(3), 217-228.
Murphy, S.V., Atala, A., 2014. 3D bioprinting of tissues and organs. Nat Biotechnol 32(8), 773-785.
Ning, L., Sun, H., Lelong, T., Guilloteau, R., Zhu, N., Schreyer, D.J., Chen, X., 2018. 3D bioprinting of scaffolds with living Schwann cells for potential nerve tissue engineering applications. Biofabrication 10(3), 035014.

Niu, C.J., Fisher, C., Scheffler, K., Wan, R., Maleki, H., Liu, H., Sun, Y., C, A.S., Birngruber, R., Lilge, L., 2015. Polyacrylamide gel substrates that simulate the mechanical stiffness of normal and malignant neuronal tissues increase protoporphyin IX synthesis in glioma cells. J Biomed Opt 20(9), 098002.
Pollard, S.M., Yoshikawa, K., Clarke, I.D., Danovi, D., Stricker, S., Russell, R., Bayani, J., Head, R., Lee, M., Bernstein, M., Squire, J.A., Smith, A., Dirks, P., 2009. Glioma stem cell lines expanded in adherent culture have tumor-specific phenotypes and are suitable for chemical and genetic screens. Cell Stem Cell 4(6), 568-580.
Quaresma, M., Coleman, M.P., Rachet, B., 2015. 40-year trends in an index of survival for all cancers combined and survival adjusted for age and sex for each cancer in England and Wales, 1971-2011: a population-based study. Lancet 385(9974), 1206-1218.
Ramos, A.R., Elong Edimo, W., Erneux, C., 2018. Phosphoinositide 5-phosphatase activities control cell motility in glioblastoma: Two phosphoinositides PI(4,5)P2 and PI(3,4)P2 are involved. Adv Biol Regul 67, 40-48.
Regot, S., Hughey, J.J., Bajar, B.T., Carrasco, S., Covert, M.W., 2014. High-sensitivity measurements of multiple kinase activities in live single cells. Cell 157(7), 1724-1734.
Reid, J.A., Mollica, P.A., Bruno, R.D., Sachs, P.C., 2018. Consistent and reproducible cultures of large-scale 3D mammary epithelial structures using an accessible bioprinting platform. Breast Cancer Res 20(1), 122.
Roseti, L., Cavallo, C., Desando, G., Parisi, V., Petretta, M., Bartolotti, I., Grigolo, B., 2018. Three-Dimensional Bioprinting of Cartilage by the Use of Stem Cells: A Strategy to Improve Regeneration. Materials (Basel) 11(9).
Rowley, J.A., Madlambayan, G., Mooney, D.J., 1999. Alginate hydrogels as synthetic extracellular matrix materials. Biomaterials 20(1), 45-53.
Sato, T., Vries, R.G., Snippert, H.J., van de Wetering, M., Barker, N., Stange, D.E., van Es, J.H., Abo, A., Kujala, P., Peters, P.J., Clevers, H., 2009. Single Lgr5 stem cells build crypt-villus structures in vitro without a mesenchymal niche. Nature 459(7244), 262-265.
Schmeichel, K.L., Bissell, M.J., 2003. Modeling tissue-specific signaling and organ function in three dimensions. J Cell Sci 116(Pt 12), 2377-2388.
Shamir, E.R., Ewald, A.J., 2014. Three-dimensional organotypic culture: experimental models of mammalian biology and disease. Nat Rev Mol Cell Biol 15(10), 647-664.
Shi, Y., Du, L., Lin, L., Wang, Y., 2017. Tumour-associated mesenchymal stem/stromal cells: emerging therapeutic targets. Nat Rev Drug Discov 16(1), 35-52.
Simian, M., Bissell, M.J., 2017. Organoids: A historical perspective of thinking in three dimensions. J Cell Biol 216(1), 31-40.
Singh, S.K., Clarke, I.D., Terasaki, M., Bonn, V.E., Hawkins, C., Squire, J., Dirks, P.B., 2003. Identification of a cancer stem cell in human brain tumors. Cancer Res 63(18), 5821-5828.
Stankevicius, V., Vasauskas, G., Bulotiene, D., Butkyte, S., Jarmalaite, S., Rotomskis, R., Suziedelis, K., 2016. Gene and miRNA expression signature of Lewis lung carcinoma LLC1 cells in extracellular matrix enriched microenvironment. BMC Cancer 16(1), 789.
Streitberger, K.J., Reiss-Zimmermann, M., Freimann, F.B., Bayerl, S., Guo, J., Arlt, F., Wuerfel, J., Braun, J., Hoffmann, K.T., Sack, I., 2014. High-resolution mechanical imaging of glioblastoma by multifrequency magnetic resonance elastography. PLoS One 9(10), e110588.
Tabriz, A.G., Hermida, M.A., Leslie, N.R., Shu, W., 2015. Three-dimensional bioprinting of complex cell laden alginate hydrogel structures. Biofabrication 7(4), 045012.
Thoma, C.R., Zimmermann, M., Agarkova, I., Kelm, J.M., Krek, W., 2014. 3D cell culture systems modeling tumor growth determinants in cancer target discovery. Adv Drug Deliv Rev 69-70, 29-41.
Tibarewal, P., Zilidis, G., Spinelli, L., Schurch, N., Maccario, H., Gray, A., Perera, N.M., Davidson, L., Barton, G.J., Leslie, N.R., 2012. PTEN Protein Phosphatase Activity Correlates with Control of Gene Expression and Invasion, a Tumor-Suppressing Phenotype, But Not with AKT Activity. Sci Signal 5(213), ra18.

Tigyi, G.J., Yue, J., Norman, D.D., Szabo, E., Balogh, A., Balazs, L., Zhao, G., Lee, S.C., 2019. Regulation of tumor cell - Microenvironment interaction by the autotaxin-lysophosphatidic acid receptor axis. Adv Biol Regul 71, 183-193.
Tykocki, T., Eltayeb, M., 2018. Ten-year survival in glioblastoma. A systematic review. J Clin Neurosci 54, 7-13.
Valkenburg, K.C., de Groot, A.E., Pienta, K.J., 2018. Targeting the tumour stroma to improve cancer therapy. Nat Rev Clin Oncol 15(6), 366-381.
Whitehead, R.H., Jones, J.K., Gabriel, A., Lukies, R.E., 1987. A new colon carcinoma cell line (LIM1863) that grows as organoids with spontaneous differentiation into crypt-like structures in vitro. Cancer Res 47(10), 2683-2689.
Xu, X., Farach-Carson, M.C., Jia, X., 2014. Three-dimensional in vitro tumor models for cancer research and drug evaluation. Biotechnol Adv 32(7), 1256-1268.
Yamada, K.M., Cukierman, E., 2007. Modeling tissue morphogenesis and cancer in 3D. Cell 130(4), 601-610.
Yuki, K., Uozumi, T., Kodama, Y., Kurisu, K., Mikami, T., 1994. In vitro chemosensitivity test of human brain tumors using a three-dimensional organ culture with a collagen gel matrix. J Neurooncol 21(3), 225-232.
Yung, W.K., Shapiro, J.R., Shapiro, W.R., 1982. Heterogeneous chemosensitivities of subpopulations of human glioma cells in culture. Cancer Res 42(3), 992-998.
Zegers, M.M., O'Brien, L.E., Yu, W., Datta, A., Mostov, K.E., 2003. Epithelial polarity and tubulogenesis in vitro. Trends Cell Biol 13(4), 169-176.
Zhao, Y., Yao, R., Ouyang, L., Ding, H., Zhang, T., Zhang, K., Cheng, S., Sun, W., 2014. Three-dimensional printing of Hela cells for cervical tumor model in vitro. Biofabrication 6(3), 035001.

Figure Legends

Fig. 1. (A) Schematic representation of 3D bioprinting with alginate. The printable bioink is prepared by mixing of cells and hydrogel matrix followed by pre-crosslinking with low concentration divalent cation exposure. The printed construct achieves stability by final crosslinking with higher divalent cation concentration. (B) The equipment used for the 3D printing experiments shows the bioprinter with the controlling computer (left) and the 8-valve syringe pump (right) driving the deposition system extruding the bioink via (C). The printer has 6 print head nozzles. All bioprinting experiments were conducted in a sterile laminar flow cabinet.

Fig. 2. Tuning of alginate stiffness influences embedded cell behaviour. (A) Representative 2% RGD-alginate constructs crosslinked calcium chloride ($CaCl_2$) for 15 min and analysed as shown in (B) and (C). (B) Representative dynamic mechanical analysis (DMA) plot. C. The stiffness comparison of constructs crosslinked with 10 mM and 50 mM $CaCl_2$. (D) Representative brightfield images of U87MG cells embedded in 2 % RGD-alginate with varying crosslinking concentration of $CaCl_2$ (top panel). Examples of extended/spread cells and rounded cells are identified with red and black arrows respectively. The zoomed images again illustrate spread and rounded cells (bottom panels). (E) Quantification of cell spreading and rounded cells from D. * = $p < 0.05$ ** = $p < 0.01$, scale bar 20 µm. Error bars: S.E.M.

Fig. 3. Recovery or protein and RNA from cells embedded in alginate. U87MG cells were suspended into 2% alginate at a concentration of 10^6 cells/mL, crosslinked with 10 mM $CaCl_2$ for 30 minutes and incubated for 24 h in complete medium. Control cells were maintained in 2D adherent culture in parallel. To block the phosphorylation of AKT, the small molecule pan-isoform inhibitor of class I PI3Ks, GDC0941/pictilisib was added to some cultures. These 3D alginate cultures were then washed with ice cold PBS and treated with 7x gel volume of the indicated concentrations of pre-chilled chelating agent to sequester divalent cations and dissolve each gel. The culture mixtures were incubated on ice for 10 minutes then centrifuged at 4°C and cell pellets lysed for the analysis of protein and RNA. Proteins were separated by SDS-PAGE and analysed either by total protein stain (A) or immunoblotting to reveal retained protein abundance and phosphorylation (B). RNA samples were analysed by standard reverse transcriptase (RT)-PCR with and without RT treatment (C) and by quantitative real-time RT-PCR (D), again with and without RT.

Fig. 4. Morphology and viability of printed cells. (A and B) U87MG-GFP cells (green) and aMM6-mCherry cells (red) were printed in (A) unmodified alginate and (B) RGDS-alginate. (C and D) U87MG cells expressing GFP show long term viability and proliferation at (C) day 1 post-printing and (D) day 26 post-printing. In (C) and (D) green fluorescent cells were printed and cell death assessed by uptake of Propidium Iodide (PI - Red). (E) shows the viability of different cell lines printed in RGD-alginate. Cells treated with the cytotoxic topoisomerase inhibitor Etoposide at 10 mM are included as a control. Mean +/- SEM. (F) shows a co-printed construct of labelled U87MG, WI38 and MM6 cells expressing three different fluorescent proteins, EYFP, Cerulean and mCherry respectively.

Fig. 5. Glioma Stem Cell (GSC) lines. (A) Viability of the GSC lines G144, G166 and G7 24 h after bioprinting assessed by propidium iodide exclusion. Mean +/- SEM. (B) Nestin and GFAP staining showing that G7 cells retain the expression of the stem cell marker Nestin even after removal of FGF and EGF. (C) G7 glioblastoma stem cells expressing mCherry (red), primary human microglia expressing GFP (green) and GASC expressing cerulean (blue) were co-printed and photographed 6 hours later. The scale bar represents 100 μm.

Fig. 6. Drug dose response of glioblastoma cells in 3D bioprinted models. U87MG or G7 cells were cultured in 2D or 3D printed in RGDS-Alginate and the were treated with increasing concentrations of either (A) cisplatin or (B) temozolomide for 72 hours. Calibration curves were included and the experiment was performed 3 times. (C) U87MG-EGFP and (D and E) G7-EGFP, were 3D printing either alone or in coculture with either MM6 cells, aMM6 cells or primary human microglia. Constructs were then treated with DMSO or temozolomide for 72 h at their respective IC50 concentrations. Viability specifically of glioblastoma cells was calculated using microscopy and Imaris software. Dead cells were stained with DRAQ7. Error bar: SEM, ANOVA analysis was performed. * $p = 0.1$, *** $p = 0.001$, n.s. = non-significant

Figure 7. Single cell kinase reporters. U87MG expressing the biosensor ERK-KTR-mClover in **(A)** prolonged 10% FBS culture (Basal - left), cultured in serum-free medium for 4 hours (middle) or with 20 % FBS for 4 hours (right). (B) The ratio between cytoplasmic and nuclear fluorescence intensity, represented in logarithmic scale for U87MG cells 3D printed in RGD alginate alone or in co-culture with MM6 and aMM6 for ERK KTR is shown. Data are represented as mean and showing the maximum and minimum values and the 25th to 75th percentile. 30 cell images were quantified for each condition using Imaris. Data are represented as the logarithm of the ratio between cytoplasm and nuclear fluorescence intensity. Difference analysed using ANOVA. * $p < 0.01$, **$p < 0.001$.

Fig. 8. Bioprinted constructs. (A) A two-layered model with a core of cancer cells surrounded by stromal cells, schematic (Left), printed construct side (middle) and from above (right). (B) A schematic of a 3 layered model, core of cancer, surrounded by mix of cancer cells and stromal cells with an exterior final layer of stromal cells (left), printed construct (middle and right). (C) 3 layer printed constructs in 12 well plate, top view (left) and side view (right). (D) U87MG cells were either plated in standard 2D adherent cell culture or 3D bioprinted with and without the induction of cell death using 10 μM etoposide. Actively metabolising cell number was assessed by resazurin reduction. The data show mean +/- SEM from 3 independent experiments.

Fig. 1

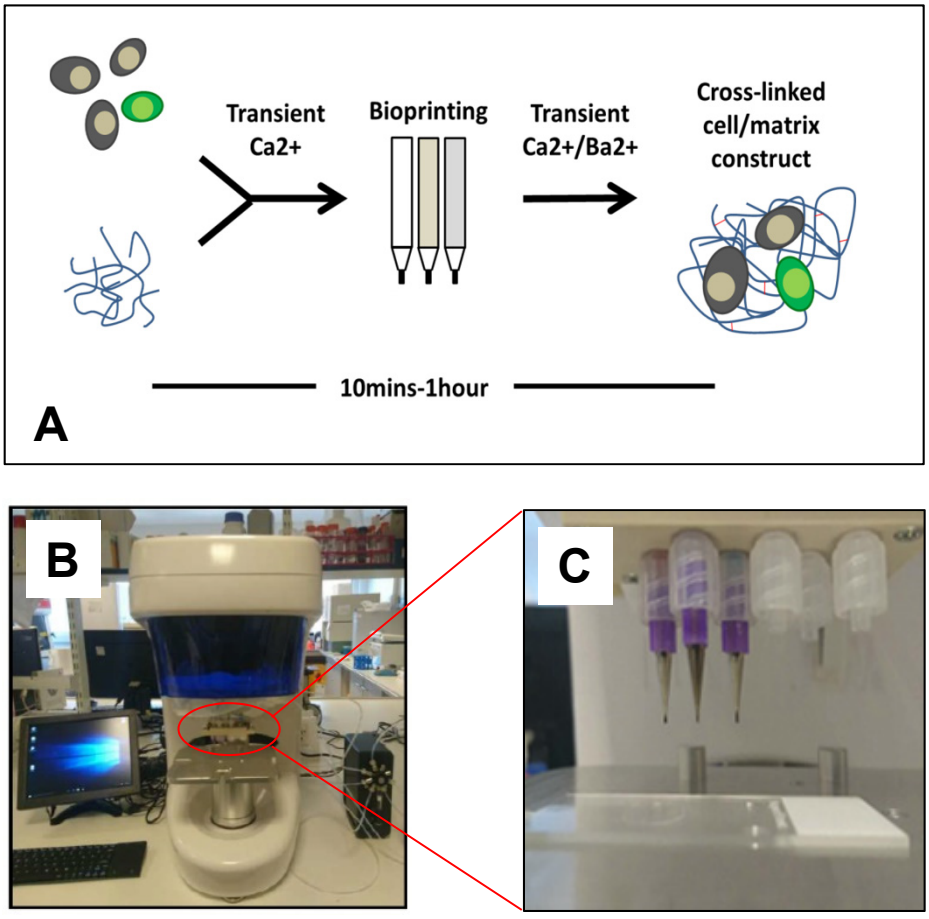
Transient
Ca2+
Bioprinting
Transient
Ca2+/Ba2+
Cross-linked
cell/matrix
construct
10mins-1hour
A
B
C

Fig. 2

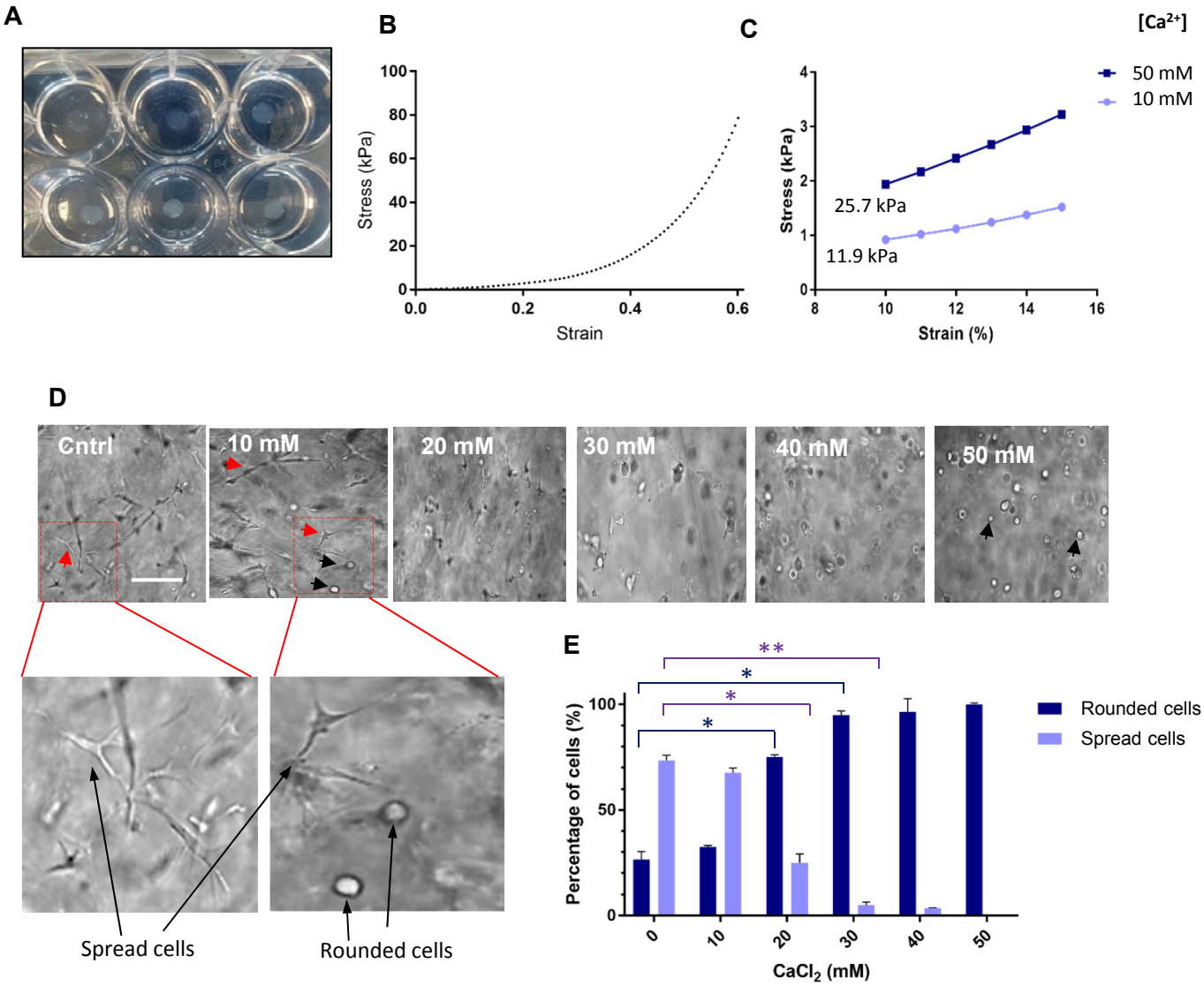
A
B
C
[Ca2+]
50 mM
10 mM
Stress (kPa)
Strain
Strain (%)
25.7 kPa
11.9 kPa
D
Cntrl
10 mM
20 mM
30 mM
40 mM
50 mM
Spread cells
Rounded cells
E
Percentage of cells (%)
CaCl2 (mM)
Rounded cells
Spread cells

Fig. 3

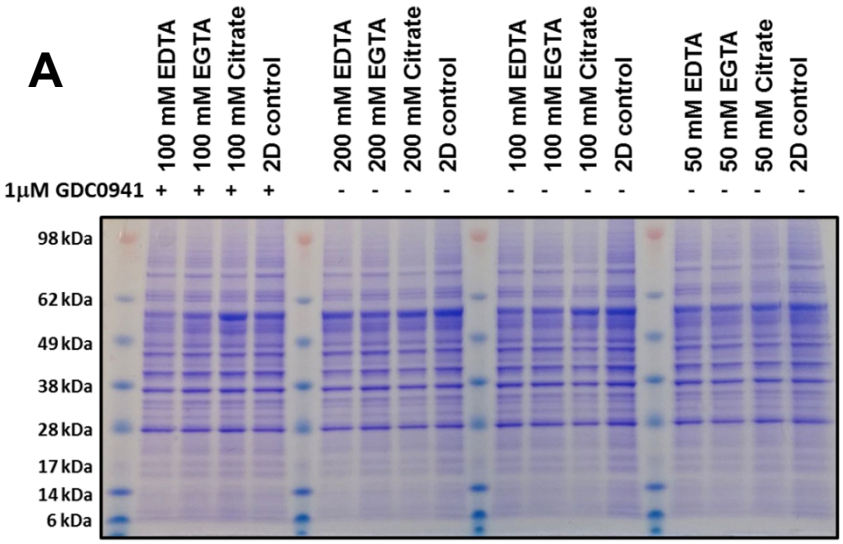
A
100 mM EDTA
100 mM EGTA
100 mM Citrate
2D control
200 mM EDTA
200 mM EGTA
200 mM Citrate
2D control
100 mM EDTA
100 mM EGTA
100 mM Citrate
2D control
50 mM EDTA
50 mM EGTA
50 mM Citrate
2D control
1μM GDC0941
98 kDa
62 kDa
49 kDa
38 kDa
28 kDa
17 kDa
14 kDa
6 kDa

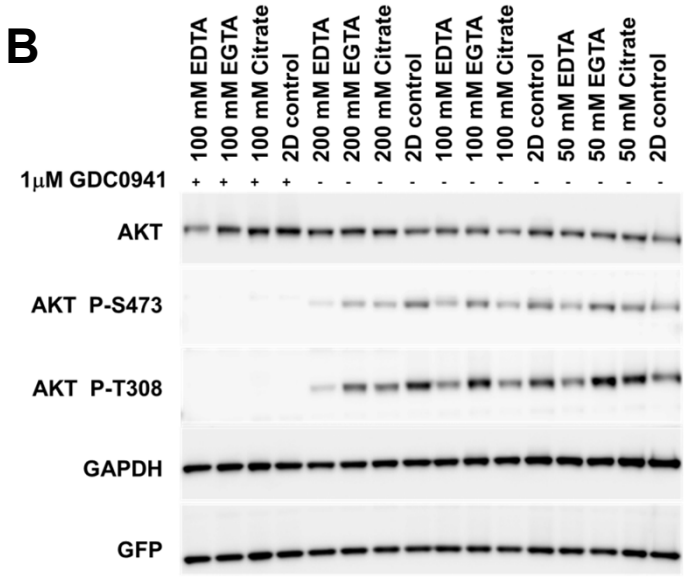
B
100 mM EDTA
100 mM EGTA
100 mM Citrate
2D control
200 mM EDTA
200 mM EGTA
200 mM Citrate
2D control
100 mM EDTA
100 mM EGTA
100 mM Citrate
2D control
50 mM EDTA
50 mM EGTA
50 mM Citrate
2D control
1μM GDC0941
AKT
AKT P-S473
AKT P-T308
GAPDH
GFP

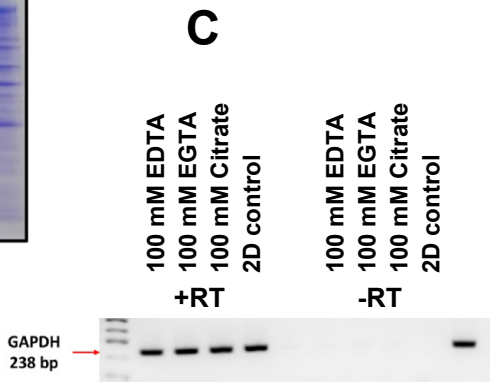
C
100 mM EDTA
100 mM EGTA
100 mM Citrate
2D control
+RT
100 mM EDTA
100 mM EGTA
100 mM Citrate
2D control
-RT
GAPDH
238 bp

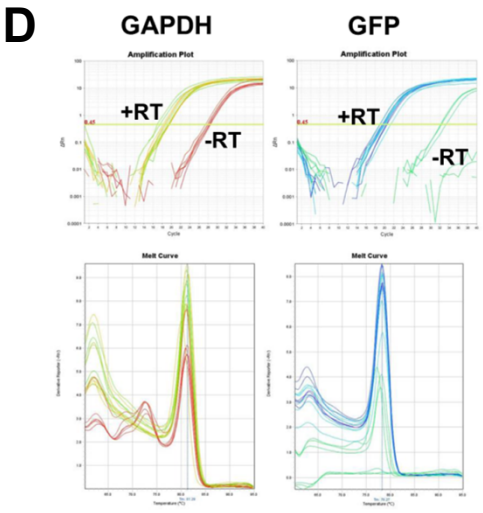
D
GAPDH
GFP
Amplification Plot
+RT
-RT
Amplification Plot
+RT
-RT
Melt Curve
Melt Curve

Fig. 4

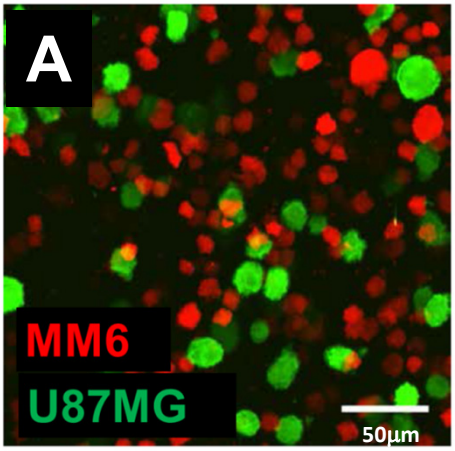
A
MM6
U87MG
50µm

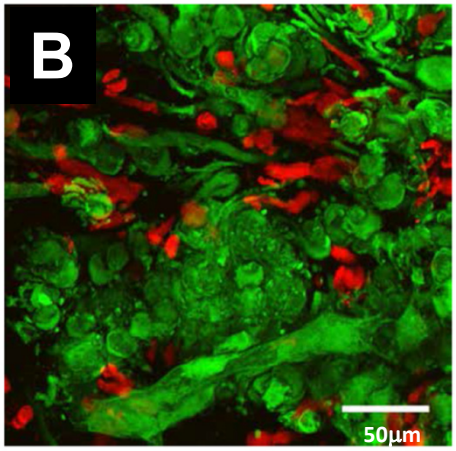
B
50µm

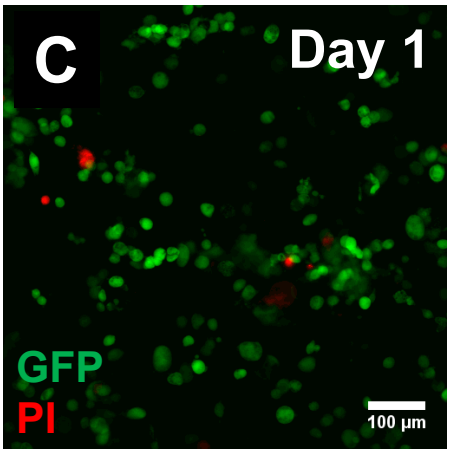
C
Day 1
GFP
PI
100 µm

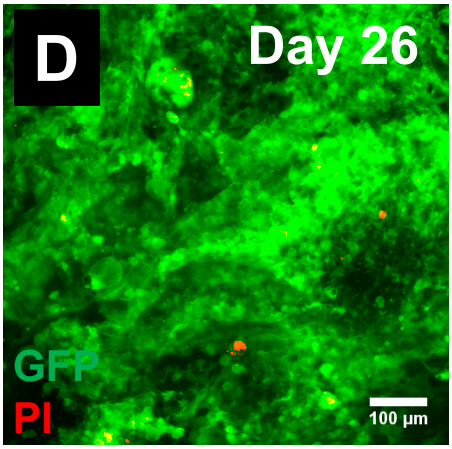
D
Day 26
GFP
PI
100 µm

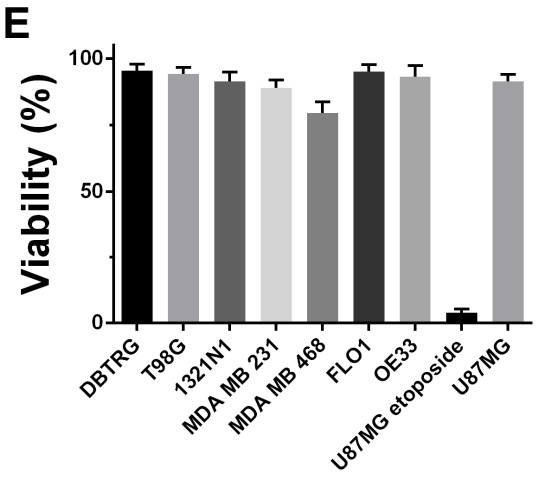
E
Viability (%)
100
50
0
DBTRG
T98G
1321N1
MDA MB 231
MDA MB 468
FLO1
OE33
U87MG etoposide
U87MG

F

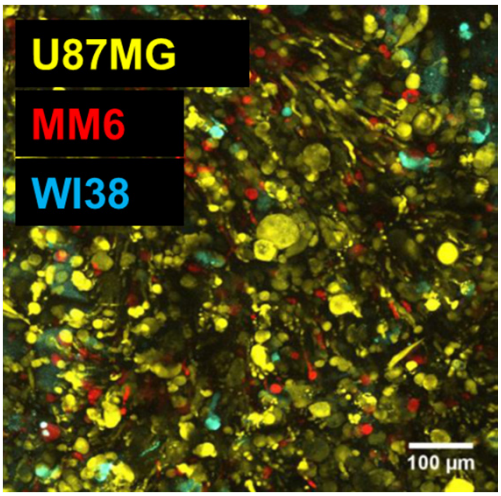
U87MG
MM6
WI38
100 µm

Fig. 5

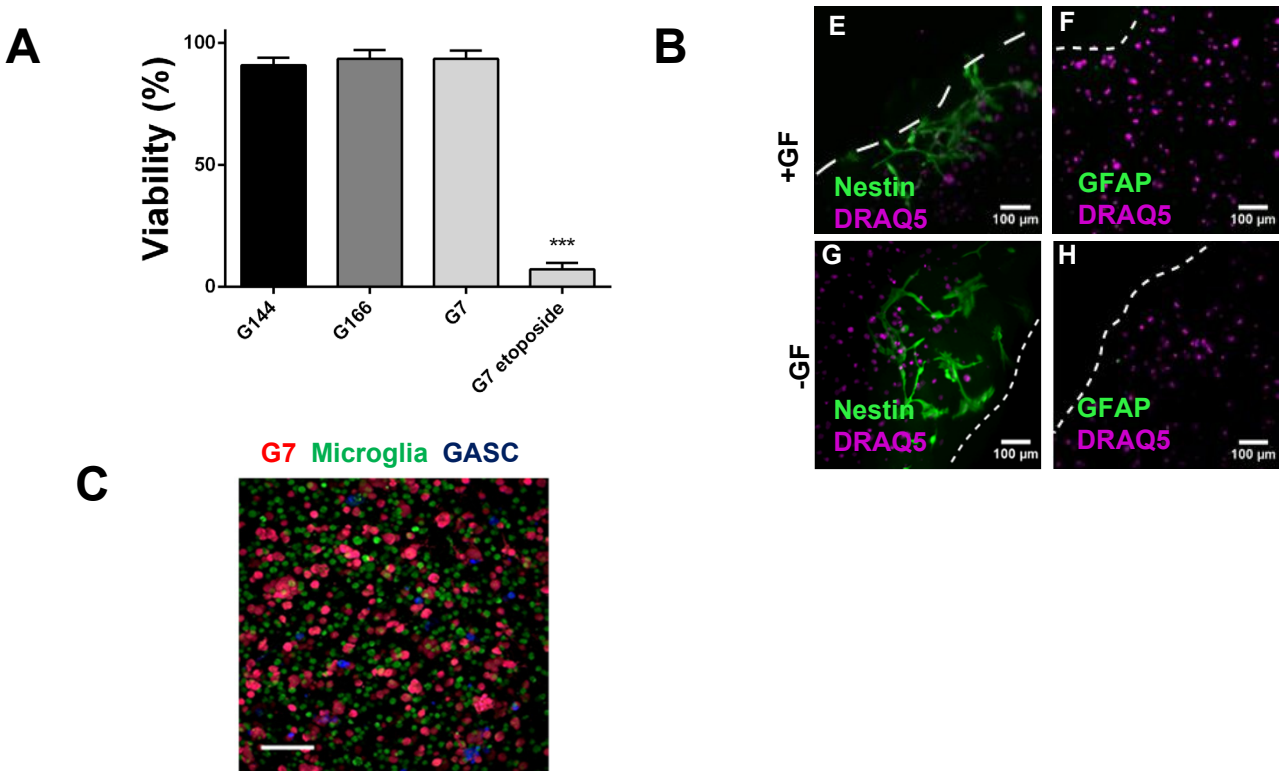
A
Viability (%)
100
50
0
***
G144
G166
G7
G7 etoposide
B
E
F
+GF
Nestin
DRAQ5
GFAP
DRAQ5
100 µm
G
H
-GF
C
G7 Microglia GASC

Fig. 6

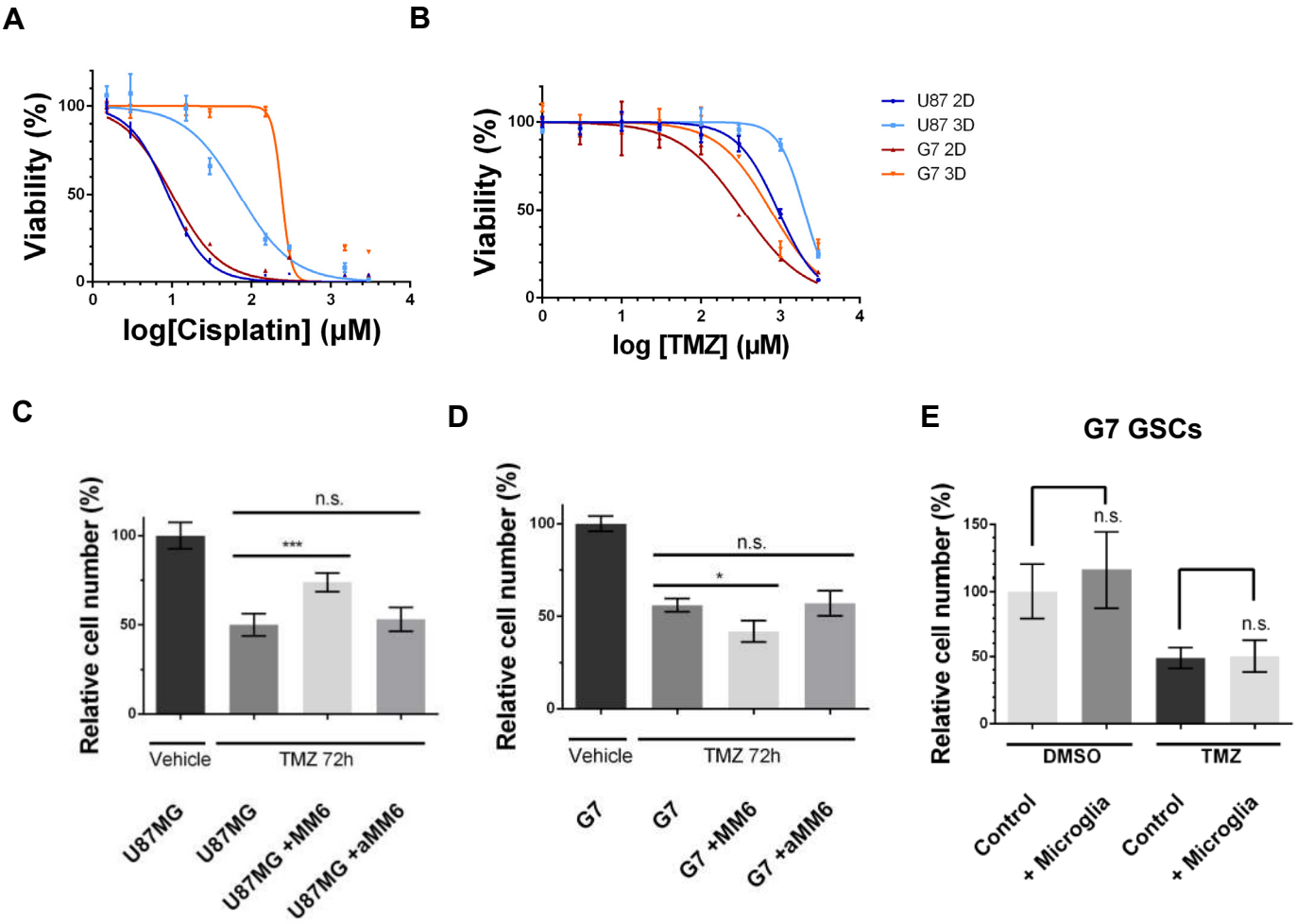
A
B
Viability (%)
log[Cisplatin] (μM)
log [TMZ] (μM)
U87 2D
U87 3D
G7 2D
G7 3D
C
D
E
G7 GSCs
Relative cell number (%)
n.s.
***
*
Vehicle
TMZ 72h
U87MG
U87MG +MM6
U87MG +aMM6
G7
G7 +MM6
G7 +aMM6
DMSO
TMZ
Control
+ Microglia

Fig. 7

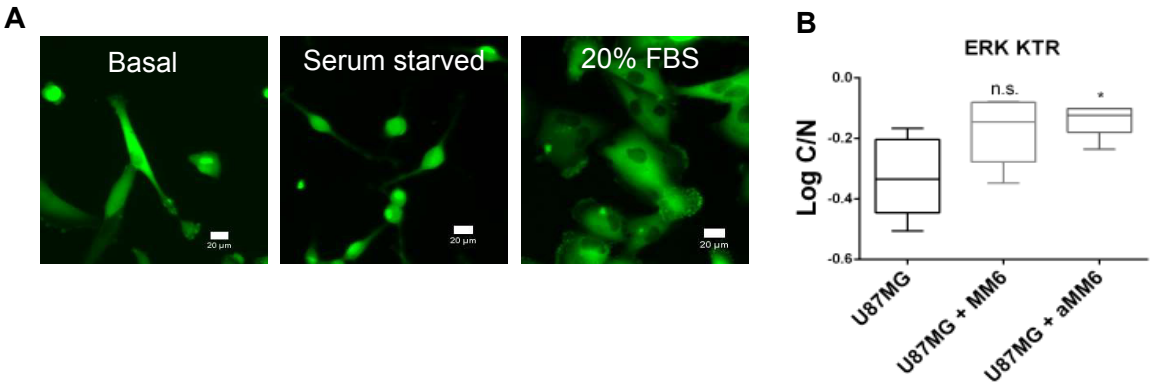
A
Basal
Serum starved
20% FBS
20 µm
B
ERK KTR
Log C/N
0.0
-0.2
-0.4
-0.6
n.s.
*
U87MG
U87MG + MM6
U87MG + aMM6

Fig. 8

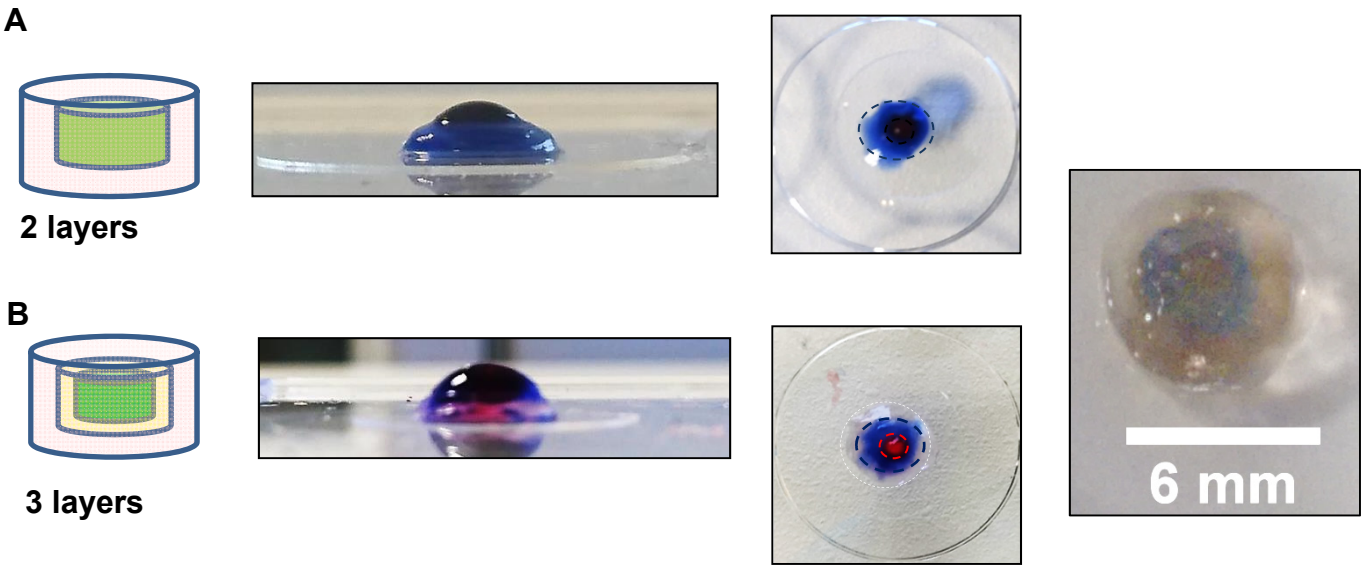
A
2 layers
B
3 layers
6 mm
3 layers
1mm/layer

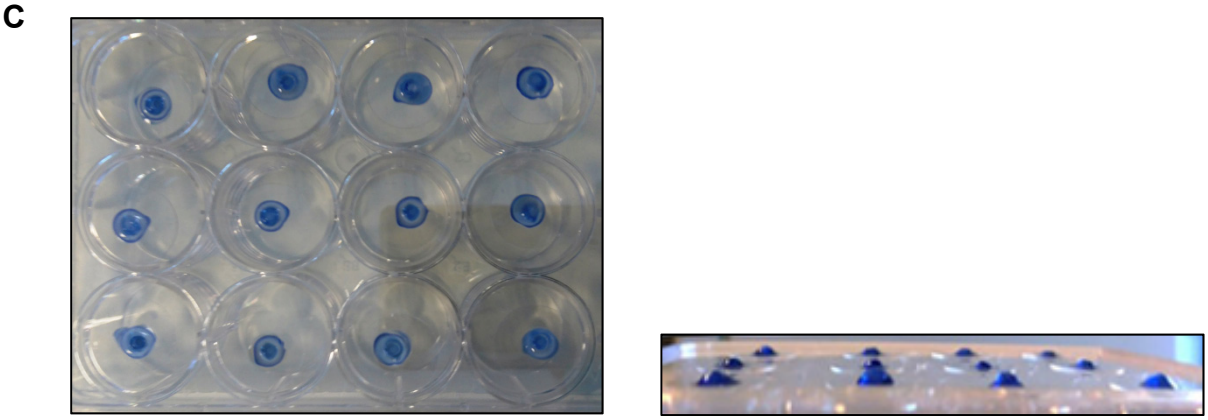
C

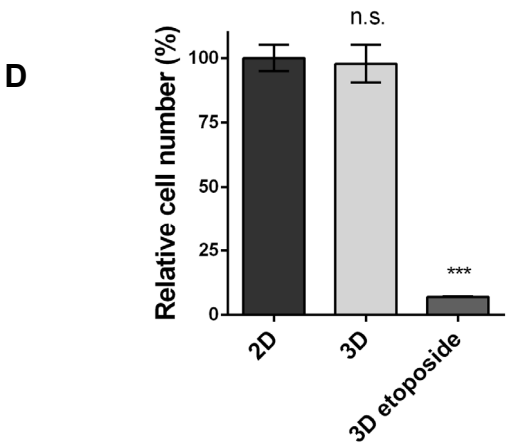
D
n.s.
Relative cell number (%)
100
75
50
25
0
***
2D
3D
3D etoposide